

Growth of (Ge,Mn) nanocolumns on GaAs(100): the role of morphology and co-doping on magnetotransport

M. Jamet¹, I.-S. Yu¹, T. Devillers¹, A. Barski¹, P. Bayle-Guillemaud¹, C. Beigne¹, J. Rothman², V. Baltz³, J. Cibert⁴

¹INAC/SP2M, CEA-UJF, Grenoble, France

²LETI/DOPT/LIR, CEA, Grenoble, France

³INAC/Spintec, CEA-CNRS-UJF, Grenoble, France

⁴Institut Néel, CNRS-UJF, Grenoble, France

(Dated: August 26, 2020)

Changing the morphology of the growing surface and the nature of residual impurities in (Ge,Mn) layers - by using different substrates - dramatically changes the morphology of the ferromagnetic Mn-rich inclusions and the magnetotransport properties. We obtained p-type layers with nanocolumns, either parallel or entangled, and n-type layers with spherical clusters. Holes exhibit an anomalous Hall effect, and electrons exhibit a tunneling magnetoresistance, both with a clear dependence on the magnetization of the Mn-rich inclusions; holes exhibit orbital MR, and electrons show only the normal Hall effect, and an additional component of magnetoresistance due to weak localization, all three being independent of the magnetic state of the Mn rich inclusions. Identified mechanisms point to the position of the Fermi level of the Mn-rich material with respect to the valence band of germanium as a crucial parameter in such hybrid layers.

PACS numbers: 75.50.Pp, 73.50.-h, 75.47.-m, 75.75.-c

Research on ferromagnetic semiconductors triggered enormous activity due to their potential use in spintronics [1, 2]. Up to now, efforts have mainly focused on diluted magnetic semiconductors (DMS) in which magnetic atoms randomly substitute the host matrix atoms [3]. Their magnetic properties can be manipulated by electric fields making them suitable materials for spintronic applications provided that they can be made ferromagnetic above room temperature. However DMS based on II-VI and III-V semiconductors still exhibit very low values of Curie temperature T_C .

Many groups have reported T_C values well above room temperature, along with remarkable magneto-transport and magneto-optical properties, in semiconductors doped with magnetic transition metals (TM). It is now admitted that these properties may be attributed to TM-rich areas resulting from spinodal decomposition [4]. Such features have been theoretically predicted [5] and reported in (Ge,Mn) [6, 7, 8, 9], and in Cr and Fe-doped GaN [10, 11] or ZnTe [12]. In this field of intense materials research, goals are now: (i) controlling spinodal decomposition to reproducibly stabilize high- T_C TM-rich areas and tailor desirable magnetic properties, and (ii) enhancing the coupling with carriers to give rise to strong magnetoresistance (MR) or anomalous Hall effect (AHE).

In this paper, we demonstrate the fine control of spinodal decomposition in (Ge,Mn) films grown on GaAs(001) substrates. We focus on (Ge,Mn) because it is compatible with mainstream silicon technology, and spinodal decomposition leads to high T_C values in layers grown on Ge substrate. Growing (Ge,Mn) films on GaAs(001) semi-insulating ($\rho > 10^7 \Omega\text{cm}$) substrates makes in-plane transport measurements easier, and constitutes a first step towards spin injection from (Ge,Mn) into a GaAs-based spin-LED [13]. Using different sur-

face preparations, we clearly identify the role of surface morphology and the role of impurity diffusion from the substrate (either Ga or As atoms), on the nanocolumns growth, on one hand, and on the electrical properties, on the other hand. We thus address the major issue of the influence of co-doping (either n-type or p-type) on spinodal decomposition in group IV magnetic semiconductors, demonstrating a major influence on the shape of the Mn-rich precipitates. We also provide new hints to control and optimize magneto-transport properties of the (Ge,Mn) films. We show that AHE and MR are not optimized simultaneously, and we propose a general picture based on the electrical doping of the matrix and on the position of Fermi level in the precipitates with respect to the valence band of Ge.

(Ge,Mn) films were grown by low temperature Molecular Beam Epitaxy (MBE), using growth conditions as described in Ref. [6], with the substrate temperature $T_g = 100^\circ\text{C}$ and deposition rate $\sim 0.2 \text{ \AA}\cdot\text{s}^{-1}$. We have used two different methods to prepare the GaAs surface. In the first one, the native oxide was thermally desorbed from an *epiready* substrate, by raising the substrate temperature up to almost 600°C . The (Ge,Mn) layers were grown directly on the resulting Ga-rich GaAs surface, which was rough as observed by RHEED. Such samples will be labelled Ga-(Ge,Mn). In the second case, As-(Ge,Mn) samples, a thin undoped GaAs buffer layer was grown first in a separate III-V system, protected with an amorphous As capping, and transferred in air to the IV-IV MBE machine. Desorbing the As capping layer at 200°C results in a very flat, (2×4) reconstructed, As-rich surface. Samples grown on Ge substrates, labelled Ge-(Ge,Mn), constitute our reference samples.

Magnetization was measured using a Superconducting QUantum Interference Device (SQUID). Magnetotrans-

port properties (magnetoresistance and Hall effect) were investigated using Hall bars defined by optical lithography, aligned along a $\langle 110 \rangle$ direction, of width $20 \mu\text{m}$, with voltage probes separated by $140 \mu\text{m}$.

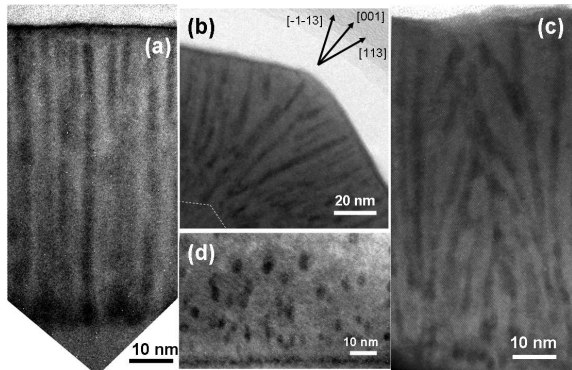


FIG. 1: TEM cross section of 80 nm thick layers : (a) $\text{Ge}_{0.94}\text{Mn}_{0.06}$ grown at 100°C after depositing a 40 nm thick Ge buffer on GaAs(001) and (b) at 100°C on the faceted Ge surface. (c) $\text{Ga-Ge}_{0.9}\text{Mn}_{0.1}$ and (d) $\text{As-Ge}_{0.98}\text{Mn}_{0.02}$ films grown at 100°C .

A typical morphology is that of long Mn-rich nanocolumns, growing normal to the substrate surface. On a Ge substrate [6] or on a Ge buffer layer grown on GaAs(001) (Fig. 1a), these nanocolumns are well aligned along the [001] growth direction. On a Ge buffer layer grown on a Ge(001) substrate with {113} facets obtained by anisotropic chemical etching in an H_2O_2 aqueous solution, Fig. 1b, they grow perpendicular to the facets. Finally, in Ga-(Ge,Mn) films, they are bent according to the initial surface roughness (Fig. 1c), and this results in a highly disordered pattern. This general picture fully agrees with 2D spinodal decomposition, driven by surface diffusion and aggregation of Mn atoms, with nucleation of Mn-rich areas taking place during the first stage of the growth [5]. As a consequence of this mechanism, the columns are always perpendicular to the growing surface.

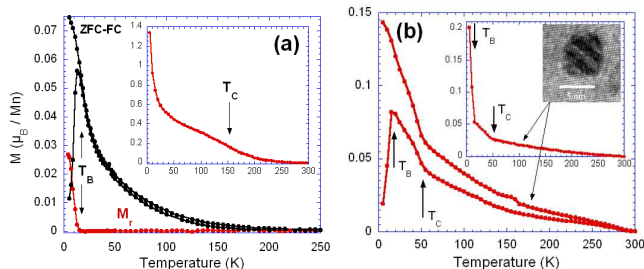


FIG. 2: Temperature dependence of magnetization in (a) $\text{Ga-Ge}_{0.9}\text{Mn}_{0.1}$ and (b) $\text{As-Ge}_{0.94}\text{Mn}_{0.06}$: ZFC-FC curves at 0.015 T and magnetic remanence M_r after maximum field cooling at 5 T. Inset: in (a), saturation magnetization at 2 T, and in (b), TEM image of a Ge_3Mn_5 cluster.

By contrast, in Fig. 1d, the As-(Ge,Mn) layers feature randomly distributed Mn-rich precipitates. In addition, a few Ge_3Mn_5 clusters already start to form, as evidenced by their typical Moiré contrast (see inset of Fig. 2b). The same random distribution of nanoclusters is observed when increasing the nominal Mn content from 2% to 6% and 10% at $T_g=100^\circ\text{C}$, but for an increase of the average precipitate density and length along the growth direction. This suggests that the decomposition is of 3D character and mostly driven by nucleation.

Secondary Ion Mass Spectroscopy (SIMS, not shown) performed on the As-(Ge,Mn) samples evidences an As-rich topmost layer, extending over 3 ± 1 nm below the sample surface and containing up to $6\times 10^{19} \text{As cm}^{-3}$, *i.e.*, an integrated amount of almost 1 ML As. This is a consequence of the segregation of As atoms, initially present at the GaAs surface, during the growth of Ge, with a well-known surfactant effect [14]. Accordingly, as described below, the As-(Ge,Mn) films appear as n-doped: As atoms are shallow donors in Ge, and in this topmost layer they compensate p-type doping by substitutional Mn.

The presence of As near the surface of the growing layer offers a possible explanation for this change of character of the spinodal decomposition, from 2D to 3D. According to Ref. [15], Mn atoms are incorporated into germanium in a subsurface interstitial position, and further diffuse within the growth plane: this offers a mechanism for 2D spinodal decomposition [5]. Codoping with As changes the charge state of Mn atoms, thus reducing Coulomb repulsion and enhancing the effect of attractive Mn-Mn pair interaction, making the nucleation of Mn-rich precipitates easier [4]. In addition to that mechanism, the presence of donors like As is expected to displace the equilibrium between interstitial Mn (another donor) and substitutional Mn (an acceptor), enhancing the amount of substitutional Mn (which form nucleation centers for further Mn aggregation [16]), and reducing the amount of interstitial Mn (thus decreasing the incorporation into already existing clusters). These different mechanisms induced by the presence of As conspire to favor a growth process dominated by nucleation, contributing to make the spinodal decomposition 3D.

A complete study of the magnetic properties will be published elsewhere [17]. All samples exhibit two [case of Ga-(Ge,Mn), Fig. 2a] or three [case of As-(Ge,Mn), Fig. 2b] magnetic phases, as evidenced from the temperature dependence of the saturation magnetization M_s (inset of Fig. 2) and the remanent magnetization M_r , and the ZFC-FC curves. They exhibit: (i) a strong paramagnetic signal with a $1/T$ temperature dependence at low temperature, attributed to Mn atoms diluted in the Ge matrix, and well fitted using a $3/2$ -Brillouin function [18]; (ii) a contribution attributed to the superparamagnetic Mn-rich nanocolumns or precipitates, with finite T_C and blocking temperature T_B ; (iii) in As-(Ge,Mn) only,

a contribution from Ge_3Mn_5 clusters with a broad range of blocking temperatures. A detailed analysis [17] of the Ga-(Ge,Mn) sample in Fig. 2a shows that $40\pm 6\%$ of the magnetic moments are in nanocolumns, with $T_C \approx 150$ K and $T_B = 15\pm 5$ K, $1.0\pm 0.1 \mu_B/\text{Mn}$, and an average magnetic moment of a nanocolumn $520\pm 50 \mu_B$. For the As-(Ge,Mn) sample in Fig. 2b, we found that $52\pm 3\%$ of the magnetic moments are in the matrix, and $22\pm 2\%$ in the Mn-rich precipitates with $T_C \approx 50$ K, $T_B=15\pm 5$ K, $1.2\pm 0.2 \mu_B/\text{Mn}$, and $\approx 100\pm 20 \mu_B$ per precipitate.

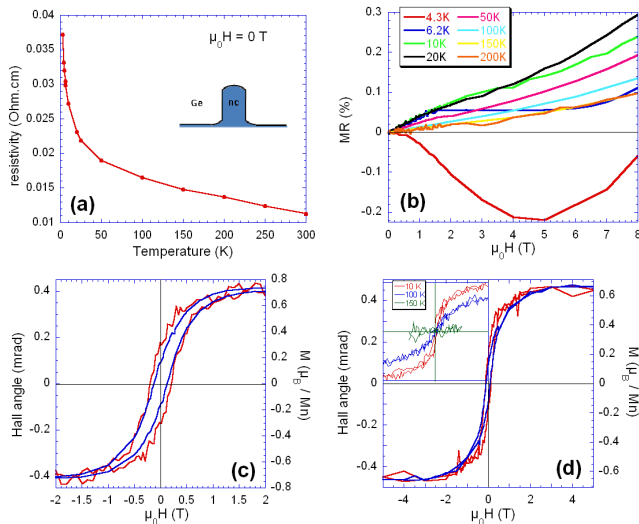


FIG. 3: Magnetotransport in Ga-Ge_{0.9}Mn_{0.1}, magnetic field applied normal to the plane: temperature dependence of the zero-field resistivity (a), MR up to 8 T at different temperatures (b), and AHE (red) compared to magnetization (blue) at 2-3 K (c) and 4-5 K (d). Inset: AHE at 10, 100 and 150 K.

From the high field slope of the Hall effect, Ga-Ge_{0.9}Mn_{0.1} films are p-type, with a hole density up to $3\times 10^{19} \text{ cm}^{-3}$ at 300 K, comparable to what we gave as a lower bound (due to a strong AHE) of the hole density in Ge-(Ge,Mn). The resistivity (Fig. 3a) is of the insulating type (it was metallic in Ge-(Ge,Mn)). Mn was reported as a double acceptor in germanium, with acceptor levels 160 meV and 370 meV above the valence band edge [19] respectively. For such a deep acceptor, the Mott critical density is expected to be well in the 10^{20} cm^{-3} range, and for a measured density one order of magnitude lower we should observe a strongly activated conductivity [20]: we actually observe (Fig. 3a) a weak temperature dependence. We conclude that the Hall effect is not due solely to the holes from the Mn acceptors in the germanium matrix. This is possible if the Fermi level of the Mn-rich material forming the precipitates lies below the top of the valence band in germanium, so that no Schottky barrier, and even an accumulation layer, is formed around each precipitate. That induces the build-up of an electric field pattern around each nanocolumn, which drags holes towards the nanocolumn.

Then the magnetotransport properties can be understood as follows: (i) as the nanocolumns configuration is well below the percolation threshold, holes have to propagate through the germanium matrix; that makes the basis of the conductivity; (ii) however, the electric field pattern drags the holes through the nanocolumns, where the conductivity is higher; applying a magnetic field suppresses this effect, creating the geometrically enhanced orbital MR, or Extraordinary MR (EMR)[21] which we observed to be strong in Ge-(Ge,Mn) [6]; (iii) finally, the absence of Schottky barrier enhances the interaction of holes with Mn atoms in the nanocolumns, thus allowing a spin polarization and a strong AHE to appear [6].

In the Ga-(Ge,Mn) samples, we still observe the EMR (Fig. 3b), with the same temperature dependence as in Ref. [6], but much weaker (although much higher than classical Lorentz MR). This is readily explained by considering the dependence of EMR on the carrier mobility (it scales as μ^2): as seen in Fig. 3a, the zero-field resistivity ρ_0 in Fig. 3a is of the order of $10^{-2} \Omega \text{ cm}$, so that the mobility is lower than in Ge-(Ge,Mn) by more than one order of magnitude, possibly due to the higher disorder and induced defects. Finally, at very low temperature, negative MR is observed, which may be due to spin disorder scattering [22] on Mn atoms diluted in the Ge matrix (as typical in metallic DMS), or to GMR on the Mn-rich nanocolumns. In both cases, this effect is expected to be very weak; in addition the spin diffusion length of holes is very short due to spin-orbit coupling, making GMR on Mn-rich nanocolumns unlikely.

AHE in Ga-(Ge,Mn) nicely matches the magnetization of the nanocolumns (Fig. 3c-d). Again, the effect is weaker than in Ge-(Ge,Mn), by almost two orders of magnitude. This is expected from the lower mobility: it was pointed out in Ref. [23] that scattering on impurities such as Ga atoms (SIMS measurements have indeed shown that Ga out-diffused from the GaAs substrate) partly suppresses the effect of skew scattering.

As-(Ge,Mn) films exhibit metallic n-type conductivity. This is clearly due to the presence of As donors in the topmost layer. Hence magnetotransport essentially measures the properties of this 3 nm thick layer. We observe no AHE, as expected since spin-orbit scattering is small for electrons in the conduction band of germanium, and also because the same assumptions as above (Fermi level of precipitates lying below the top of the valence band) creates a high Schottky barrier for electrons.

MR is highly anisotropic (Fig. 4a): we show now that this is due to 2D weak localization in the As-doped layer, which vanishes when the field is applied in-plane ($\theta = 0$). The isotropic part (Fig. 4c-d) will be analyzed later on.

The MR of non-interacting electrons in the 2D weak localization regime is $\Delta\rho/\rho \approx -\Delta\sigma/\sigma = -A \cdot f_2[4e\mu_0 H \sin(\theta) L_\phi/\hbar]$ [24], where $A = e^2/2\pi^2\hbar\sigma_{2D}(0)$, L_ϕ is the phase relaxation length, and the function $f_2(x)$ is defined in [24]. Here we neglect

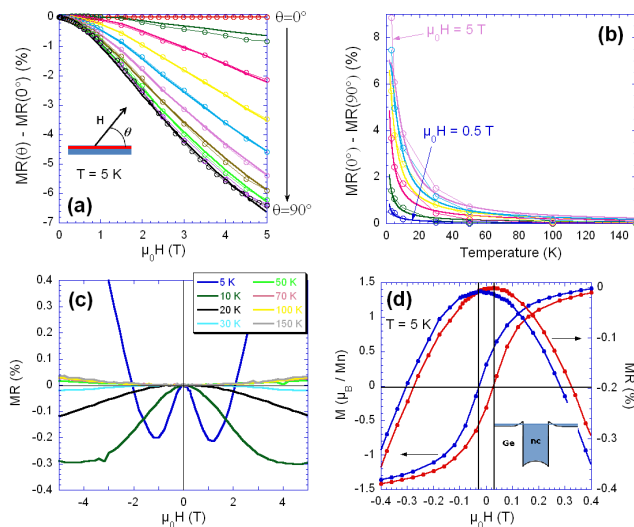


FIG. 4: Magnetotransport in As-Ge_{0.94}Mn_{0.06}. (a) field dependance and (b) temperature dependence of the MR anisotropy, for different orientations of the field; symbols are experimental data, solid line calculated. (c,d) MR and magnetization as a function of the field applied in-plane.

the effect of spin-orbit coupling and the anisotropy of L_ϕ [17]. Fits in Fig. 4a were obtained with only two adjustable parameters: $A = 4\%$, close to the value $A = (6 \pm 2)\%$ calculated using the experimental value of the 2D conductivity at $H = 0$, and $L_\phi = 11.5$ nm, large enough with respect to the thickness of the conducting layer to justify the use of the 2D regime of weak localization. Moreover, fits of the temperature dependence of the anisotropic MR (Fig. 4b) were obtained by simply writing $L_\phi = \sqrt{D\tau_\phi}$, using the temperature dependence of the diffusion coefficient D for an n-doped degenerate semiconductor [25], and a temperature dependence of the phase relaxation time $\tau_\phi \propto T^{-\alpha}$ with $\alpha \approx 1.7$, similar to that obtained in [26] for Ge:Sb ($\alpha=1.5$) and in [27] for Si-MOSFETs ($\alpha=1.6$), and currently attributed to both electron-electron and electron-phonon collisions.

Turning back to the isotropic MR, Fig. 4c-d, it contains a negative contribution, which features two maxima at the coercive field of Mn-rich precipitates, and vanishes above 50 K as does their magnetization. Hence, we tentatively ascribe it to tunneling MR (TMR) through the precipitates and the Schottky barriers formed around them. By analogy with spin injection from a ferromagnetic metal to a semiconductor [28], efficient spin injection from the precipitate to the matrix requires an interface resistance provided by the Schottky barrier. This barrier must be high enough to prevent full spin relaxation inside the precipitate but reasonably transparent to allow tunnel MR to occur.

To summarize, we have shown that surface morphol-

ogy and co-doping have major influence on spinodal decomposition in (Ge,Mn) films grown on GaAs(001) substrates. For films grown on Ga-rich rough surfaces, we recovered 2D spinodal decomposition with bent nanocolumns. Electrical properties are similar to what we obtained on Ge(001) substrates except that the presence of defects in the films leads to weaker positive MR and AHE. For films grown on As-rich flat surfaces, 3D spinodal decomposition is observed due to As co-doping and magnetotransport is dominated by TMR and weak localization, AHE is negligible. These results are consistent with the assumption that the Fermi level of Mn-rich precipitates lies in the valence band of the Ge matrix.

We thank A. Arnault (LAAS, Toulouse) for providing As-capped GaAs substrates, T. Dietl and J. Pernot for fruitful discussions. This work was granted by the Agence Nationale pour la Recherche (project GeMO) and the Nanoscience Foundation in Grenoble (project IMAGE).

-
- [1] A. H. MacDonald *et al.*, Nature Mater. **4**, 195 (2005).
 - [2] T. Dietl *et al.*, Semicond. Sci. Technol. **17**, 377 (2002).
 - [3] H. Ohno *et al.*, Science **281**, 951 (1998).
 - [4] T. Dietl *et al.*, J. Appl. Phys. **103**, 07D111 (2008).
 - [5] K. Sato *et al.*, Jpn. J. Appl. Phys. **44**, L948 (2005).
 - [6] M. Jamet *et al.*, Nature Mater. **5**, 653 (2006).
 - [7] D. Bougeard, S. Ahlers, A. Trampert, N. Sircar, G. Abstreiter, Phys. Rev. Lett. **97**, 237202 (2006).
 - [8] A. P. Li *et al.*, Phys. Rev. B **75**, 201201(R) (2007).
 - [9] T. Devillers *et al.*, Phys. Rev. B **76**, 205306 (2007).
 - [10] L. Gu *et al.*, J. Magn. Magn. Mater. **290-291**, 1395 (2005).
 - [11] A. Bonanni *et al.*, Phys. Rev. Lett. **101**, 135502 (2008).
 - [12] S. Kuroda *et al.*, Nature Mater. **6**, 440 (2007).
 - [13] R. Fiederling *et al.*, Nature **402**, 787 (1999).
 - [14] A. Leycuras *et al.*, Appl. Phys. Lett. **66**, 1800 (1995).
 - [15] W. Zhu *et al.*, Phys. Rev. Lett. **93**, 126102 (2004).
 - [16] W. Zhu, Z. Zhang, E. Kaxiras, Phys. Rev. Lett. **100**, 027205 (2008).
 - [17] I.-S. Yu *et al.*, to be published.
 - [18] T. C. Schulthess *et al.*, J. Appl. Phys. **89**, 7021 (2001).
 - [19] H. H. Woodbury *et al.*, Phys. Rev. **100**, 659 (1955).
 - [20] P. Achatz *et al.*, Appl. Phys. Lett. **92**, 072103 (2008).
 - [21] S. A. Solin *et al.*, Science **289**, 1530 (2000).
 - [22] F. Matsukura, H. Ohno, A. Shen, Y Sugawara, Phys. Rev. B **57**, R2037 (1998).
 - [23] Y. D. Park *et al.*, Science **295**, 651 (2002).
 - [24] B. L. Altshuler and A. G. Aronov, in *Electron - Electron Interactions in Disordered Systems*, edited by A. L. Efros and M. Pollak (North-Holland, Amsterdam, 1985), p. 1.
 - [25] S. M. Sze, *Physics of Semiconductors Devices* (Wiley, New York, 1981).
 - [26] T. A. Polyanskaya *et al.*, Sov. Phys. JETP Lett. **34**, 361 (1981).
 - [27] M. J. Uren *et al.*, J. Phys. C **14**, L395 (1981).
 - [28] A. Fert and H. Jaffrès, Phys. Rev. B **64**, 184420 (2001).